Quantitative imaging of a non-combusting diesel spray using structured laser illumination planar imaging

**E. Berrocal · E. Kristensson · P. Hottenbach ·
M. Aldén · G. Grünefeld**

Abstract Due to its transient nature, high atomization process, and rapid generation of fine evaporating droplets, diesel sprays have been, and still remain, one of the most challenging sprays to be fully analyzed and understood by means of non-intrusive diagnostics. The main limitation of laser techniques for quantitative measurements of diesel sprays concerns the detection of the multiple light scattering resulting from the high optical density of such a scattering medium. A second limitation is the extinction of the incident laser radiation as it crosses the spray, as well as the attenuation of the signal which is to be detected. All these issues have strongly motivated, during the past decade, the use of X-ray instead of visible light for dense spray diagnostics. However, we demonstrate in this paper that based on an affordable Nd:YAG laser system, structured laser illumination planar imaging (SLIPI) can provide accurate quantitative description of a non-reacting diesel spray injected at 1,100 bar within a room temperature vessel pressurized at 18.6 bar. The technique is used at $\lambda = 355$ nm excitation wavelength with 1.0 mol% TMPD dye concentration, for simultaneous LIF/Mie imaging. Furthermore, a novel dual-SLIPI configuration is tested with Mie scattering detection only. The results confirm that a mapping of both the droplet Sauter mean diameter and extinction coefficient can be obtained by such

complementary approaches. These new insights are provided in this article at late times after injection start. It is demonstrated that the application of SLIPI to diesel sprays provides valuable quantitative information which was not previously accessible.

1 Introduction

The reduction of both fuel consumption and pollutants emission from diesel combustion engines is an important challenge which requires a deeper understanding of the diesel spray formation and its structure. Several trends related to the optimization of diesel combustion can be noticed. At present, the common rail direct fuel injection technology has been largely improved with regard to injection pressure (up to 3,000 bar), flexibility of the injector (piezo systems), and changes in nozzle design (smaller orifices). Modern piezo injectors enabled the engineers to use shorter injection durations, multiple-injection strategies, and injection-rate shaping. The number of orifices in a nozzle has increased up to a certain limit (8 for high speed direct injection (HSDI) [1]) whereas the nozzle hole has decreased to diameters around 100 μm. Thus, the mixture formation process has shifted from a global-flow-controlled state to an injection-controlled state [1]. Substantial improvements with regard to engine performance, fuel consumption, and emissions were achieved in this way. This evolution in diesel combustion technology confirms the importance to further understand the liquid fuel atomization process and air–fuel mixture formation. More specifically, the end of the injection event is becoming more relevant due to the application of relatively short injection durations, multiple-injection, and retarded combustion [2, 3]. It was demonstrated, for instance, that

E. Berrocal (✉) · E. Kristensson · M. Aldén
Division of Combustion Physics, Lund University,
P.O. Box 118, SE-221 00 Lund, Sweden
e-mail: edouard.berrocal@forbrf.lth.se

P. Hottenbach · G. Grünefeld
Institute for Laser Diagnostics in Thermo-Fluid Dynamics,
RWTH Aachen University, Schinkelstr. 8,
52062 Aachen, Germany
e-mail: gruenefeld@ltfd.rwth-aachen.de

there may be a strong interaction between consecutive injections for a multiple-injection strategy under engine-like conditions in a vessel [3]. Heatable high-pressure vessels are often used for detailed optical investigations, because the optical access is easier and the ambient-air conditions are controlled more accurately than in an optical engine. Over the past two decades, a variety of optical diagnostics have been developed and tested within high-pressure vessels to further understand and characterize diesel sprays. A short review of these techniques is given below.

1.1 Laser sheet imaging for diesel spray diagnostics

Owing to the creation and extensive use of laser sheet based techniques, during the nineties, large progress could be made to obtain measurements in turbulent flows. One typical example is the well-referred conceptual model of direct injection diesel combustion which was derived in 1997 by Dec, from laser sheet imaging data [4]. At that time, laser sheet imaging became the preferred technique for diesel spray analysis, due to its capability in providing 2D spatially resolved information [5]. Particular attentions were given to the measurement of fuel mass distribution using fuel planar laser-induced fluorescence (LIF) [6] and of the droplet Sauter mean diameter (SMD) from the LIF/Mie ratio [7]. Nevertheless, even though planar imaging demonstrated great new capabilities, the detection of the multiple light scattering was quickly recognized as the main source of errors [8, 9] strongly limiting quantitative diagnostics. In the early years 2000, it was believed that the LIF/Mie ratio might partly cancel out the multiple light scattering intensity detected on both images allowing denser sprays to be probed [9]. However, this assumption is not valid and laser sheet droplet sizing of dense sprays suffer from large inaccuracies. A typical error is the observation of large droplets on one side of the spray, the entrance of the laser sheet, and small droplets on the other side, and the exit of the laser sheet. This phenomenon is demonstrated in Fig. 1 for the case of a homogeneous medium containing monodisperse dyed particles of 15 μm in diameter (results based on data published in [10]). From this observation, it can be stated that the accuracy of experimental absolute SMD results, published in the past for the characterization of dense sprays, remains questionable.

1.2 Line-of-sight techniques for diesel spray diagnostics

In order to face issues related to multiple scattering, planar laser imaging was "replaced," around 2005, by a series of new line-of-sight techniques named, Ballistic Imaging (BI)
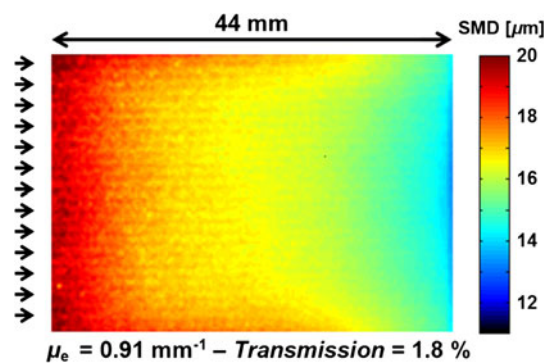
Fig. 1 Planar LIF/Mie ratio of a cuvette containing a homogeneous water solution of monodisperse scattering and fluorescing polystyrene spheres. Particles of 15 μm diameter are probed at number density 253 particles/mm³. These results clearly highlight errors introduced by multiple scattering in the LIF/Mie sizing technique. Even though the particles are monodisperse, large sizes are measured at the *entrance side* of the laser sheet while small particle are observed at the *exit side*

[11–13], X-ray absorption [14–16], X-ray phase-contrast [17, 18], and infrared double extinction [19, 20]. Note that these techniques have all been well recognized by the spray community over the past years. BI is capable of large image contrast enhancement thanks to its state-of-the-art picosecond time gate [11]. Such short temporal gate enables to reject the late photon arrivals which are responsible for image blurring. One successful application of BI in diesel spray is the clear visualization, at early time of injection, of ligaments dynamics and breakups at the liquid–gas interfaces [13]. The use of X-rays instead of visible light aims to reduce the scattering of the incident radiation for analyzing the absorption through the spray. Based on this concept, X-ray absorption was found to be particularly useful for quantitative measurement of fuel mass and phase transition [14, 15]. As the technique remains based on single point detection, it lacks the possibility of direct 2D visualization. Large number of measurements and data post-processing are then required to extract image matrices. Alternative to X-ray absorption, a phase-contrast approach has been experimented to offer the possibility of generating single-shot spray images with good spatial resolution and image contrast. The technique is adequate for the analysis of air/liquid boundaries [16], as well as, for visualizing the needle motion inside a nozzle tip [17]. Even though X-ray phase-contrast images present unique features, they can be particularly difficult to interpret in situations involving dense clouds of droplets [18], making direct correlations to fluid mechanics phenomena challenging. Finally, another interesting, but less known approach, is the infrared double extinction technique [19, 20]. The diagnostic is able to provide both SMD and Liquid Volume Fraction (LVF). The originality in using far-infrared instead of visible light is the possibility of strongly

reducing the scattering cross section of the small droplets (<10 μm at 9.27 μm wavelength) making the spray less optically dense. However, in the case of large droplets (>10 μm at 9.27 μm wavelength), this advantage is no longer valid. Note that the technique also remains a single point measurement due to the limitation of having 2D detector at these wavelengths.

1.3 Multiple light scattering suppression using SLIPI

In all line-of-sight configurations described above, the properties of the incident beam (wavelength, direction, polarization, and pulse duration) are employed to either filter out the undesired signal or reduce the optical depth of the probed spray. Due to the difficulty in extracting only singly scattered photons for side-scattering detection, where time-gating schemes or the use of non-visible light are hardly applicable, laser sheet imaging has remained, for a long time, uncorrected from multiple scattering issues, despite some attempts [8]. However, since 2008 a side-scattering approach called structured laser illumination planar imaging (SLIPI) [21] has revealed efficient capabilities in removing light intensity introduced by multiply scattered photons leading to significant image contrast enhancement.

In this article, SLIPI is used, for the first time, for the quantitative study of a non-reacting diesel spray injected at 1,100 bar within a room temperature vessel pressurized at 18.6 bar. The article first focuses on a comparison between conventional laser sheet and SLIPI Mie images to analyze the efficiency of multiple scattering suppression. Then, SMD measurements based on the ratio LIF/Mie are shown. Finally, the unique capability of measuring the extinction coefficient using a novel approach called dual-SLIPI [22] is demonstrated.

2 Structured laser illumination planar imaging

The method is based on using a laser sheet with a sinusoidal intensity pattern along the vertical direction. While the origin of multiply scattered light is mostly independent of the modulation pattern, the position of the first scattering events remains entirely faithful to it. This implies that the amplitude of the modulated component is a direct signature of the single light scattering. Figure 2 shows the reduction of this modulation amplitude between position (a) and (b), when a modulated laser sheet is crossing a homogeneous scattering medium. The SLIPI process consists in extracting, at each position along the direction of light propagation, the modulation amplitude of the laser sheet. This is performed by recording several modulated images (an example of a modulated image is shown in Fig. 2) where
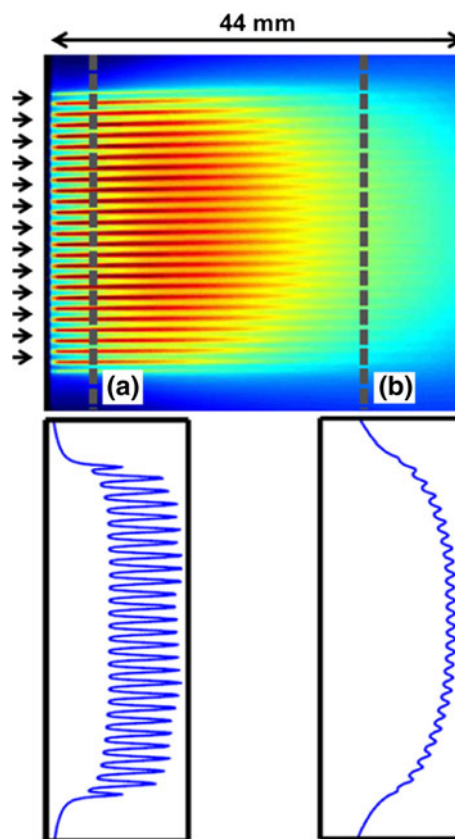
Fig. 2 Averaged Mie image of a modulated laser sheet crossing a cuvette of 15 μm polystyrene spheres in distilled water. Due to multiple light scattering, the amplitude of the modulation decreases between position (a) and (b). SLIPI aims to measure this amplitude [10]

the modulation is vertically shifted between each recording. In the referred examples [10, 21, 22], the resultant SLIPI image was reconstructed by means of three modulated images. However, the technique can be generalized to a larger number n of modulated images [23]. By vertically shifting the incident modulation $(n - 1)$ times, a series of n modulated images I are recorded with a spatial phase shift of the modulation equal to $\Delta\Phi = 2\pi/n$. The resulting SLIPI image S is then constructed according to

$$S = \frac{\sqrt{2}}{n}\left[\sum_{j=1}^{n-1}\sum_{k=j+1}^{n}\left(I_j - I_k\right)\right]^{1/2} \qquad (1)$$

where I_j and I_k are intensity values from the modulated images and the subscript j and k denotes the different image recordings. In this equation, the pair-wise subtraction $(I_i - I_j)$ removes similar features (introduced by the diffuse light) while unique features (from the directly scattered light) are kept. Note that this equation is valid to extract the amplitude of the modulation only if $n \geq 3$. This implies that a minimum of three images must be experimentally recorded to operate the SLIPI process using Eq. (1). Note

that it is possible to extract the SLIPI image from a single modulated image, but at a cost of losses in image resolution, as shown in [24].

If, however, the n images are averaged, the conventional image C is reconstructed.

$$C = \frac{1}{n} \sum_{j=1}^{n} I_j \qquad (2)$$

In the case of independent scattering (which is the case for spray systems), C equals the image acquired using a homogeneous (non-modulated) laser sheet. Therefore, by comparing C to S the amount of multiple scattering intensity rejected by the SLIPI filtering can be quantified. Examples of SLIPI and conventional images extracted using Eqs. (1) and (2), respectively, are shown in Fig. 3 for both LIF and Mie detection. These results have been
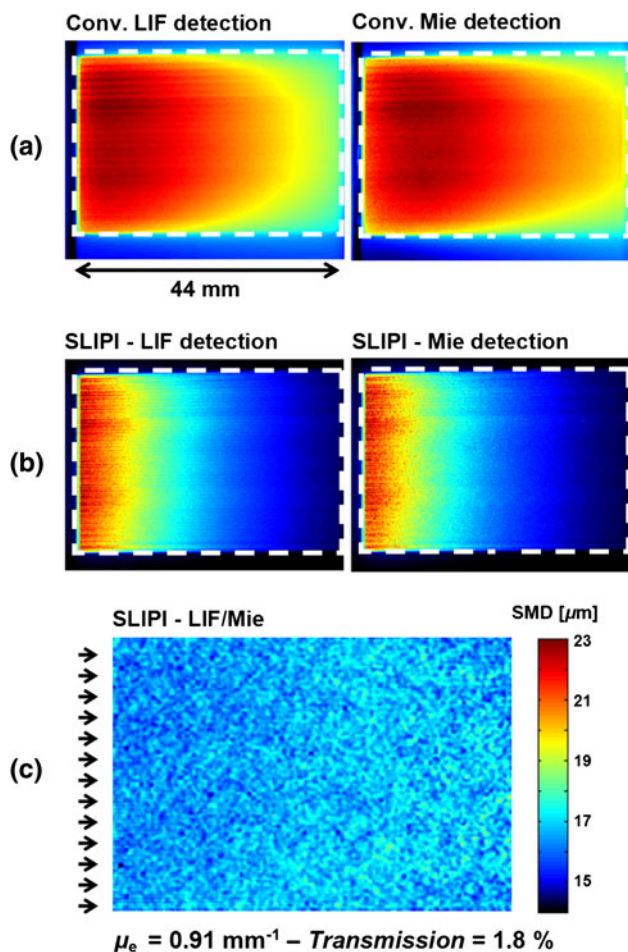
Fig. 3 Comparison between conventional planar imaging in (**a**) and SLIPI in (**b**) for Mie and LIF detection (data from [10], with permission). Here, a water solution containing scattering dyed spheres of 15 µm, at number density 253 particles/mm³ is probed. As seen from (**c**) the resultant SLIPI-LIF/Mie image shows a near constant SMD over the entire image, in opposition to the conventional ratio presented in Fig. 1

extracted from [10] and the same scattering medium shown in Figs. 1 and 2 is probed here. By suppressing the multiple light scattering intensity, the extinction of the laser sheet along its incident direction can now be observed on the SLIPI images as shown in Fig. 3b. Furthermore, the LIF/Mie ratio is faithful to the monodisperse nature of the probed medium, with a quasi-constant SMD measured over the whole field of view (Fig. 3c). These first results demonstrate the importance of using SLIPI for correct LIF/Mie droplet sizing in sprays.

3 Experimental set-ups

In this work, a non-combusting diesel spray is injected in a three optical accesses pressurized vessel (details of the vessel can be found in [25]). The fuel injection is operated by a modern common rail injector (Bosch type piezo 3G) equipped with a three-hole nozzle, each of 105 µm in diameter. The rail pressure is set to 1,100 bar. The energizing time of the injector is 850 µs. Injection starts at about 0.2 ms after the onset of the energizing time [26]. Figure 6 shows that the end of the quasi-steady injection phase (when the needle starts closing) is reached between 1,500 and 2,000 µs after start of injection, when the measured signals start to decrease. Hence, it is significantly delayed with regard to the end of the energizing time. This is consistent with [26], in which the injection system was characterized by conventional optical techniques. This hydraulic delay is explained in more detail in [27]. The air in the vessel is at ambient temperature $\sim 20\ °C$ and pressurized up to 18.6 bars. Here, n-decane is used, as it is a commonly employed surrogate for standard diesel fuel. Images are acquired by two intensified CCD cameras (ICCD-Nanostar, 1280 × 1024 pixels). A prototype of the SLIPI instrument developed by LaVision is used to create the desired intensity modulated laser sheet (with a sinusoidal pattern) to accurately shift the phase of the modulation and to operate the required image post-processing. SLIPI and conventional images are reconstructed based on three modulated images, where the modulation of the laser sheet is successively shifted by a third of the period between the recordings. A complete description of the SLIPI optical set-up with detailed explanations regarding how the modulated laser sheet is formed and vertically shifted can be found in Ref. [23].

The spray is illuminated at $\lambda = 355$ nm using the third harmonic of a Nd:YAG laser system. The formed modulated laser sheet is 35 mm height, ~ 500 µm thin at the center of the spray and with a spatial period of the modulation of 400 µm. Two detection strategies, based on averaged imaging, were considered in this work. The aim of the first set-up is to visualize spray evolution at various

times after injection and to apply SLIPI droplet sizing from simultaneous Mie and LIF recordings. The second set-up is based on Mie scattering only, but imaged on both sides of the laser sheet. This configuration allows the measurement of extinction coefficient. A description of the respective setups and related diagnostics is given below.

3.1 Set-up for simultaneous SLIPI-LIF/Mie

When applied under correct conditions [28–30], the LIF signal generated by a dye doped droplet gives a direct measure of the droplet volume whereas the elastically scattered light from Mie scattering represents the droplet surface area. Dividing the LIF signal by the Mie for a distribution of droplets, the SMD is deduced as

$$\text{SMD} = \frac{K_{\text{LIF}}}{K_{\text{Mie}} \cdot Q_{\text{s}}} \frac{\int\limits_{D=0}^{\infty} D^3 \cdot \mathrm{d}N(D)}{\int\limits_{D=0}^{\infty} D^2 \cdot \mathrm{d}N(D)} \quad (3)$$

where $\mathrm{d}N(D)$ is the probability distribution of the droplets and Q_{s} is related to the angle of detection relative to the incident direction. K_{LIF} and K_{Mie} include experimental factors such as scattering efficiency, detector response, signal collection solid angle, laser power, etc. Usually, the ratio $K_{\text{LIF}}/(K_{\text{Mie}} \cdot Q_{\text{s}})$ is assumed to be a constant for a given system and is experimentally deduced after calibration (using, for instance, Phase Doppler Anemometry). However, this assumption is not valid (especially at 90° detection [29]) and the theory suggests using a calibration curve instead of a constant [27]. Recent numerical calculation on the accuracy of the LIF/Mie ratio for droplet sizing, based on pure single scattering, can be found in [29, 30], where the accuracy of the technique is investigated for a large range of refractive index, absorption coefficient (related to the dye concentration), detection angle, and spread of the droplet size distribution. In addition to uncertainties calculated numerically, several experimental problems remain. As a result, extracting the absolute SMD using LIF/Mie is not an easy task and requires knowing some important parameters, making a number of assumptions and following an adequate procedure. This can be described as follows:

- Knowing the real and imaginary parts of the droplet refractive index.
- Knowing the real and imaginary parts of the surrounding medium.
- Assuming a droplet size distribution with a given spread. Note that different spreads and shape of droplet distribution results in different numerical calibration curves. This induces errors on the resultant mean SMD.

- Numerically calculating an adequate calibration curve considering the experimental detection conditions of the collecting lens.
- Experimentally calibrating the system.
- Assuming that the spray is not evaporating and that the LIF signal from the gas phase is negligible.
- Assuming that the detected signal originates from single light scattering.

The work presented in this article focuses on this last important point. It should be remarked that any effort in accurately calibrating via experiment and/or simulation a LIF/Mie signal is a vain effort if there is no guaranty that the experimental measurement is performed in the single scattering regime [31] or if the light intensity from multiple scattering is not suppressed. The inaccuracy of planar droplet sizing induced by the detection of multiple light scattering is demonstrated in Fig. 1, where a monodispersed distribution of scattering spheres cannot be observed. By suppressing this unwanted light intensity contribution using SLIPI a more accurate SMD mapping is obtained, as demonstrated in Fig. 3. The histograms of the image data presented in Figs. 1 and 3c are shown in Fig. 4b and d, respectively. Here, a calibration constant was assumed in the case of 7 μm particles shown in Fig. 4a and c, and used for the 15 μm particles. These results demonstrate that even a measure of the relative SMD is not reliable when multiple light scattering is detected. From this observation, it is evident that before focusing on absolute quantitative SMD, a fundamental investigation of the possibility in extracting, at least, the relative SMD by means of SLIPI should first be investigated.

A description of the experimental set-up for simultaneous detection of the LIF and Mie signals is depicted in Fig. 5. For this configuration, TMPD (tetramethyl-p-phenylene diamine) dye is added to the *n*-decane fuel at 1.0 mol% concentration, as recommended by Kamimoto [32]. A band pass filter centered at 355 nm and a 355 nm long pass filter are used to detect the Mie scattering and the LIF, respectively. Imaging at various times, from 100 up to 4,000 μs, after injection start is performed to obtain a statistical time sequence of the spray development as illustrated in Fig. 6. Based on this time sequence, the development of the spray can be analyzed either from the LIF or from the Mie images. Each of the modulated images used to reconstruct the conventional and SLIPI images is averaged over 30 single shots, imaging 30 independent injections. The LIF/Mie ratio is calculated only at late time after injection starts, corresponding to 2,000, 2,500, and 3,000 μs, when the droplets are spherical and do not undergo further breakups. In this case good statistics are required and an averaging over 100 single-shots for each

Fig. 4 Histogram comparison of the SMD calculated from the LIF/Mie ratio with conventional planar imaging in (**a**) and (**b**), and SLIPI in (**c**) and (**d**). Histograms (**b**) and (**d**) are extracted from the images presented in Figs. 1 and 3c, respectively. Histograms (**a**) and (**c**) present a similar case of study but for 7 μm spheres. It is observed that the measurement of the particle size distribution whith SLIPI shows a much more realistic monodisperse distribution
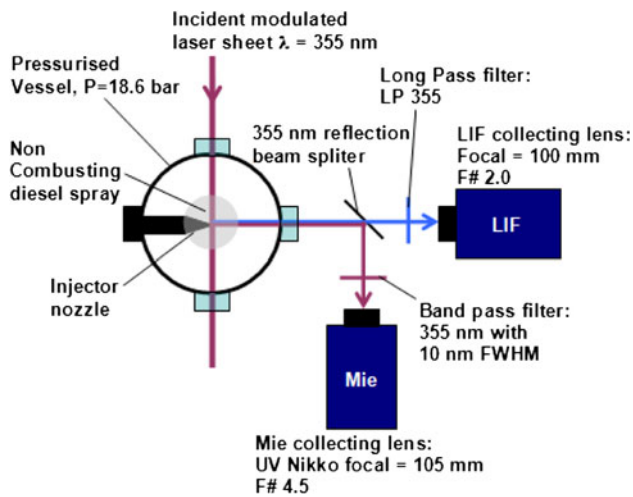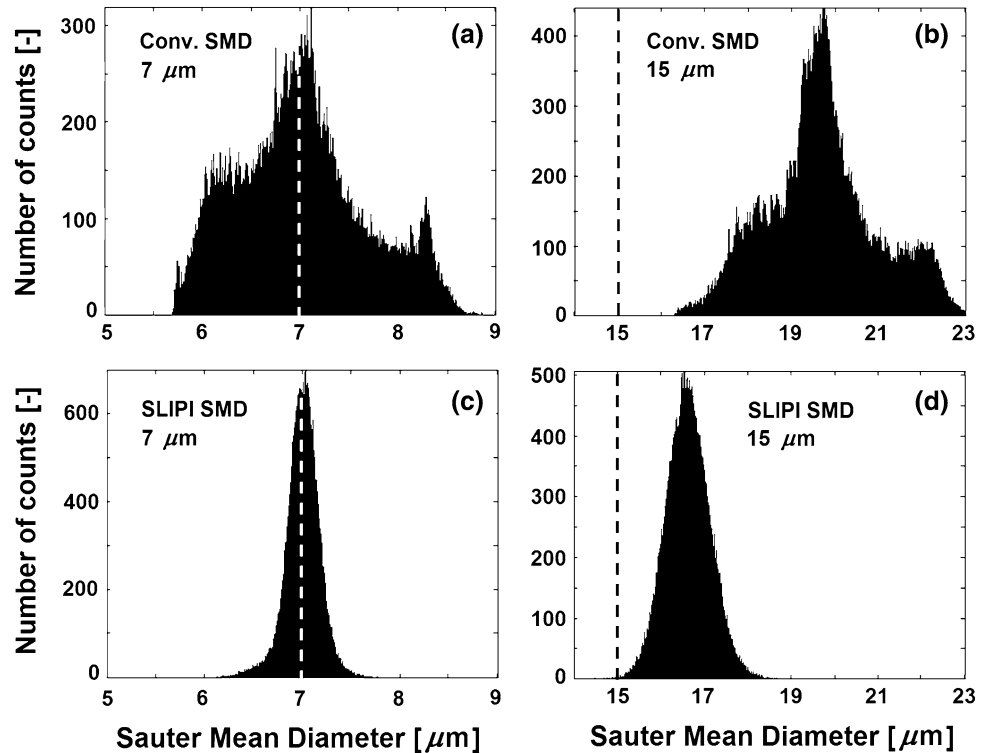
Fig. 5 Detailed description of the experimental setup for simultaneous LIF/Mie detection

modulated image is operated (300 images in total are, in this case, used to reconstruct a single SLIPI image).

3.2 Set-up for dual-SLIPI

The main goal of dual-SLIPI, described in [22], is to extract the extinction coefficient in-between two respective positions of the laser sheet. For each position, the laser sheet is imaged on both sides, by means of two cameras as illustrated in Fig. 7. As a result four SLIPI images, $S_{(P1,C1)}$,

$S_{(P1,C2)}$, $S_{(P2,C1)}$, and $S_{(P2,C2)}$ are recorded where the subscripts P1 and P2 correspond to positions 1 and 2 while C1 and C2 correspond to camera 1 and 2, respectively. By means of these four SLIPI images and by applying the Beer–Lambert relation, remaining effects due to laser extinction and signal attenuation are accounted for. The measurement of the extinction coefficient between the two positions of the laser sheet in the spray (separated by a distance Δz) is finally obtained as

$$\mu_e = \ln\left(\frac{S_{(P1,C1)} \cdot S_{(P2,C2)}}{S_{(P2,C1)} \cdot S_{(P1,C2)}}\right) \cdot \frac{1}{2\Delta z} \qquad (4)$$

Detailed derivation of Eq. (4) and description of the technique is given by Kristensson et al. [22]. The main advantage of this novel approach is to easily correct for laser extinction and signal attenuation without performing transmission measurement and applying a post-processing algorithm for 3D reconstruction as shown in [23]. Note that these effects are also accounted for in the SLIPI-LIF/Mie ratio as the extinction cross section of the droplets remains similar between $\lambda = 355$ nm (Mie scattering) and $\lambda_{peak} \sim 390$ nm (fluorescence). No dye is added for the dual-SLIPI measurement as only Mie scattering is recorded. The two cameras must have an identical detection acceptance angle, and single scattering radiation is supposed to scatter equally on both sides of the laser sheet. This assumption of symmetrical scattering is valid for spherical droplets. Similar to the SMD determination an averaging over 100 single-shots for each modulated image

Fig. 6 Time sequence of a non-combusting diesel spray generated at 1,100 bar injection pressure within a vessel pressurized at 18.6 bars. A comparison between conventional laser sheet imaging and SLIPI is shown for the detection of Mie and LIF signals. Thanks to the filtering process operated by SLIPI, almost only single light scattering is detected. For *each column*, the light intensity is normalized to the maximum intensity value detected at 100 μs after injection start. The *arrows* indicate the entrance side of the laser sheet
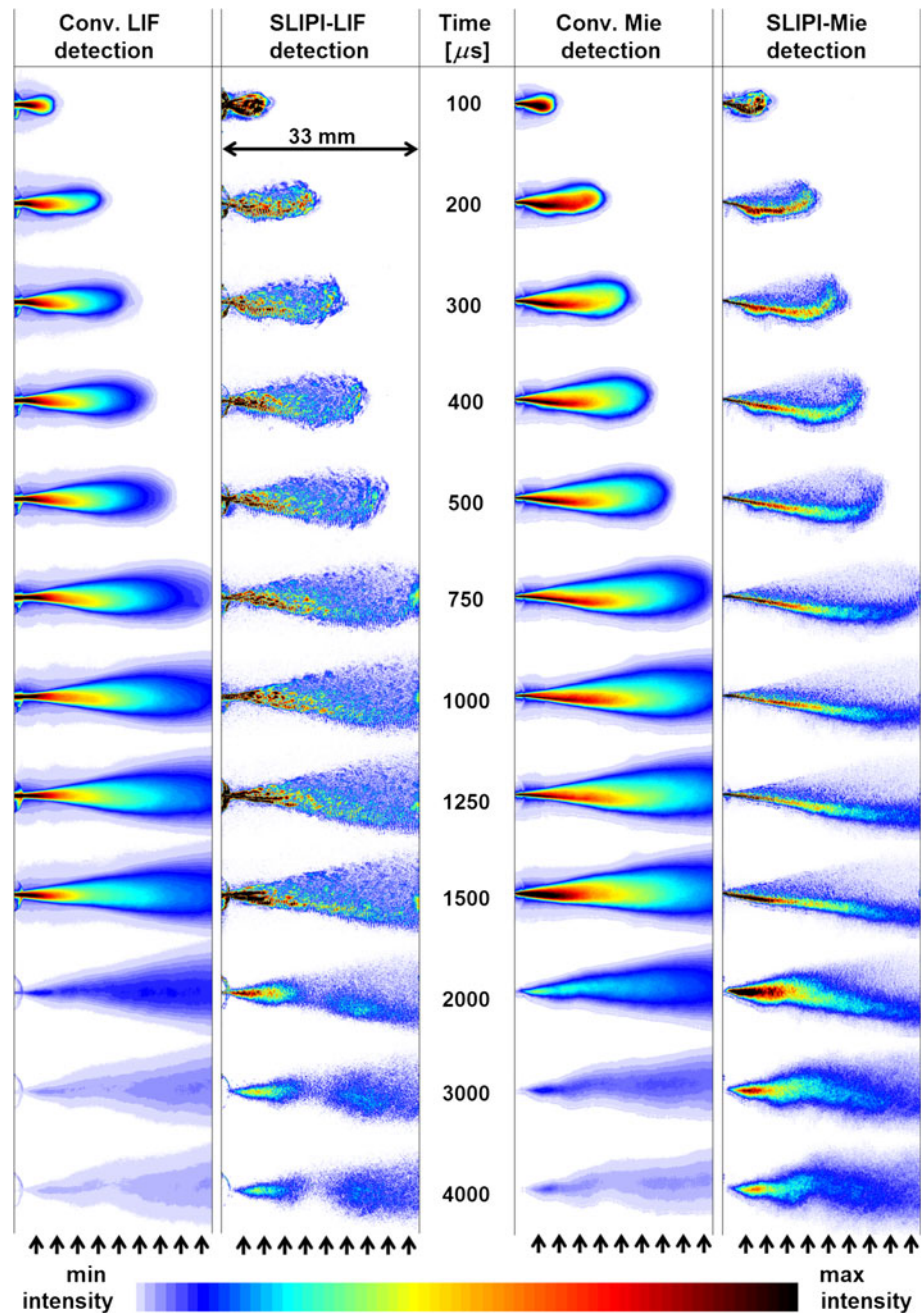
is operated at 2,000, 2,500, and 3,000 μs after injection starts.

4 Assessment of multiple scattering suppression

As observed, in Fig. 3, for a homogeneous medium, the multiple scattering suppression offered by SLIPI allows the observation of light extinction as the laser sheet crosses the medium. Similar effects can be visualized in the diesel spray, as shown from the SLIPI image sequences given in Fig. 6 for both the Mie and LIF. However, due to the polydisperse and highly inhomogeneous nature of the diesel spray, the combined effect of laser extinction and signal attenuation is complex and cannot be easily predicted. The resultant light energy losses are clearly visible in the SLIPI images where the laser sheet seems to not penetrate the spray fully. Such phenomenon tends to be less important later in the injection event when the spray becomes more dilute. The main assumption used in quantitative measurements of sprays is that all photons reaching the detector should have encountered only one scattering event. This single scattering assumption is not the case in conventional planar image. One important remaining
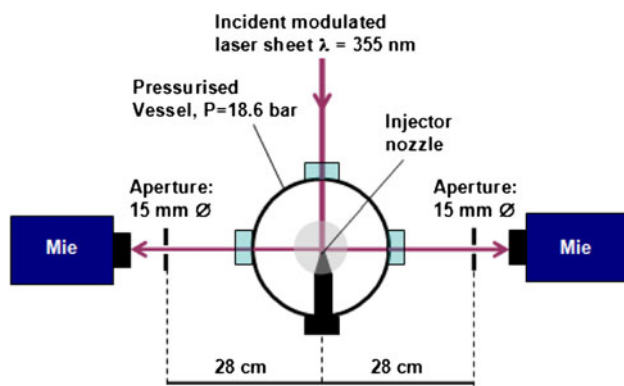
Fig. 7 Detailed description of the experimental setup for dual-SLIPI Mie detection

question concerns, then, the efficiency of SLIPI in removing the multiple scattering intensity contribution. Some preliminary answers were obtained by means of numerical Monte Carlo simulation, demonstrating that up to 91 % of the multiple scattering suppression could be reached [33], for a given modulation frequency. In this case, the simulated spray had similar scattering properties

(e.g., optical depth, refractive indices, and droplet size) than a non-combusting diesel spray. Complementary experimental evaluation of the SLIPI efficiency in multiple scattering suppression can be found in [10] for homogeneous scattering media. The published results confirm that the SLIPI image provides a very close signature of the singly scattered light, which, in our case of study, originates from the illuminating laser sheet. On the contrary, the conventional image contains both single and multiple scattering intensities as explained above. So by dividing the SLIPI to the conventional image, a 2D visualization of the amount of single light scattering contained in the conventional image can be estimated. This ratio is shown in Fig. 8 for the detection of the Mie scattering at various times after the injection start.

It is observed that the largest amounts of single light scattering intensity correspond to the entrance side of the laser sheet in the spray. The maximum values are observed at the latest times (3,000–4,000 μs) and approximately equals 35 %. Note, however, that at the very early injection time 100 μs, the tip of the spray also shows strong single light scattering intensity. This observation can be explained
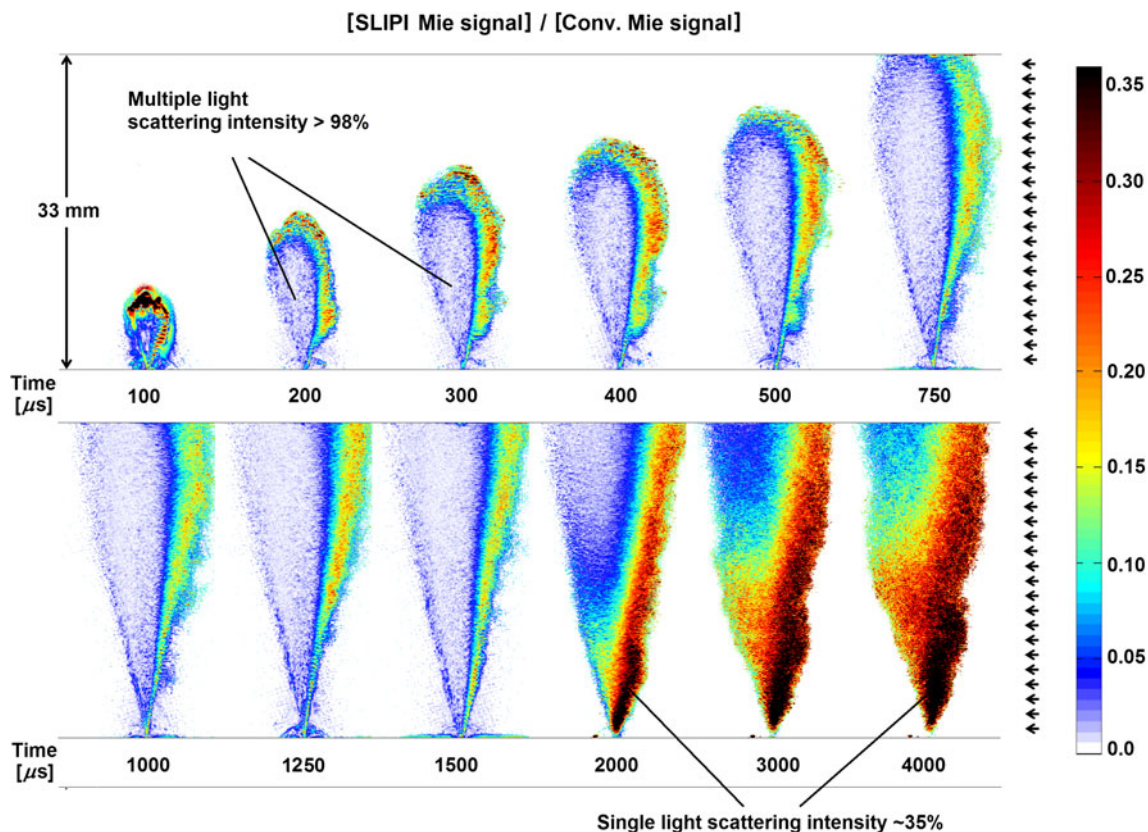
Fig. 8 Time sequence of the ratio of the SLIPI images over the Conv. image for the Mie scattering detection (see the *right side* of Fig. 6). These images are a representation of the amount of single light scattering detected in conventional imaging. At best only ∼35 % of the light, which is located at the entrance of the laser sheet in the

spray, at late time after injection, is singly scattered. These results demonstrate both the inadequacy of conventional planar imaging for quantitative measurement in diesel sprays and the efficiency of SLIPI to reject this undesired light. The *arrows* indicate the entrance side of the laser sheet

by the fact that a portion of light is directly reflected to the camera, by the first large liquid bodies penetrating the surrounding air. The lowest amount of single light scattering detected is inferior to 2 % and is located in the central and left side where the laser sheet exits the spray. This minimum value is observed at each time sequence between 200 and 2,500 μs. Such results demonstrate the inadequacy of using conventional planar imaging for quantitative spray measurement in non-combusting diesel sprays, as more than 65 % of multiple light scattering is usually detected. These results strongly support the use of SLIPI instead.

5 Quantitative results and discussion

Similar to the previous section, one spray plume generated by the three-hole injector is illuminated and investigated here. Results corresponding to the LIF/Mie ratio using the set-up described in Fig. 5 are given in Fig. 9. Spray

evolution at late times, 2,000, 2,500, and 3,000 μs after injection start, are considered.

Due to the reasons explained in "Set-up for simultaneous SLIPI-LIF/Mie," the relative (and not the absolute) distribution of the droplet SMD in the central region of the spray is shown in Fig. 9. In (a) the SMD image corresponding to the conventional detection is presented. Similar to the case of the homogeneous scattering medium presented in Fig. 1, larger droplets seem to be located on one side of the spray, at the entrance the light sheet, while smaller droplets are located on the other side, where the light sheet exits the spray, creating a non-realistic asymmetric spray structure. These initial results confirm the statement made in the previous sections regarding the inaccuracy of the conventional LIF/Mie sizing technique, even at late time after injection start. In Fig. 9b the same measurement is performed, but using SLIPI filtering. In this case, the ratio shows a more symmetrical spray structure with some strong inhomogeneities in droplet sizes along the vertical direction. Such an observation, accessible here

Fig. 9 Two-dimensional mapping of the non-reacting diesel spray at late time after injection start (between 2,000 and 3,000 μs), showing the distribution of the relative droplet SMD calculated from Conv.-LIF/Mie in (**a**) and SLIPI-LIF/Mie in (**b**). This comparison demonstrates the possibility, with SLIPI-LIF/Mie, of observing the appearance of large droplets generated due to the effect of the needle closing. Note that the spray is illuminated from the *right side*
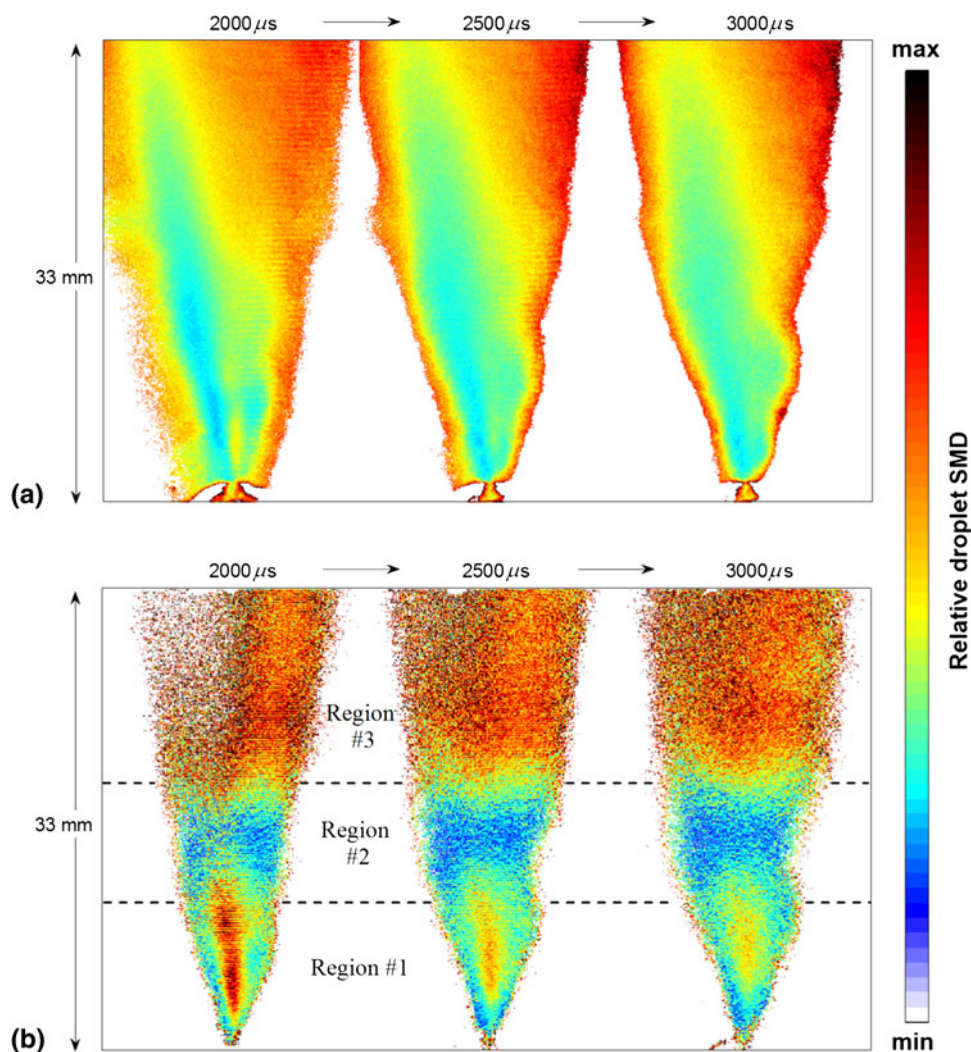
from the SLIPI data only, is precious information to characterize the performance of diesel injection systems. As shown in Fig. 9b, relatively large droplets are observed in the lower one-third of the three images, denoted region #1, corresponding to the near-nozzle region. In contrast, smaller droplets occur close to the center of the images, i.e., in region #2. Even further downstream, the SMD increases again in the upper half of the images, which denoted region #3. Interestingly, a very similar axial SMD profile was previously measured using the infrared (IR) double extinction technique [20], as shown in the lower subimage in Fig. 12 of that article (although the profile is somewhat shifted downstream there). However, it should be noted that IR measurements close to the nozzle (i.e., in the range up to 15 mm) were not presented in [20], due to the diagnostic problems discussed previously. These previous measurements were conducted in the early "spray-dissipation" phase, which is comparable to the results presented in Fig. 9b. This is a major reason for the remarkable similarity of the current and previous results, indicating that the needle closing process is accurately characterized by these measurements.

Previous radially resolved SMD measurements in earlier phases of diesel injection showed that larger droplets were located at the periphery of the sprays [5] (and references therein). This is not observed in Fig. 9b. Similarly, the IR measurements in [20] show that the radial gradients of the SMD diminish toward the end of injection. (However, "hollow-cone" sprays may occur at the very end of injection, which is not investigated in the present work, but it was visualized by rather conventional imaging techniques in [34].) The axial distribution of the SMD depicted in Fig. 9b could be explained as follows:

One might think that relatively small droplets in region #2 are caused by breakups and further downstream coalescence leads to large droplets in region #3, as suggested in a similar situation in [35] (and references therein). However, a review of more recent research reported that breakups likely occur very close to the nozzle and that the role of secondary atomization by aerodynamic shear is far less significant than previously thought [5]. Recall that region #2 is found remote from the nozzle. Thus, the axial SMD distribution consistently shown in Fig. 9b can be potentially explained by an alternative mechanism, which was discussed in [36–38]. These previous studies also demonstrated that the SMD increases with increasing nozzle distance. In this mechanism, small and large droplets are spatially separated by the aerodynamic drag effect. Thus, larger droplets are found further downstream (region #3) than smaller ones (region #2). In this picture, it is also plausible that the axial distribution of the fuel mass may not be uniform. Indeed the SLIPI–LIF images in Fig. 6, which represent the averaged fuel mass distribution, show

that the mass is lower in region #2 compared to both adjacent regions, #1 and #3, in the range 2,000–4,000 μs after start of injection. This could be further investigated by velocity measurements within the spray using laser flow tagging [39].

Furthermore, Fig. 9b shows that the SMD in region #1 decreases in the course of the needle closing process. According to [5], the droplet diameter in diesel sprays depends primarily on the diameter of the nozzle and the velocity of the jet. For instance, drop size measurements by laser diffraction demonstrated that the SMD decreased as the orifice diameter decreased [40]. According to [41], this could be explained by the increasing discharge velocity produced by decreasing orifice size, which is of prime importance to the atomization process. Thus, Fig. 9b indicates that the observed behavior can be explained by the increase of the jet velocities due to needle closing. Apparently, additional throttling of the in nozzle flow does not occur in the investigated range of the nozzle-shutoff process. Note that the droplet SMD in diesel sprays generally increases strongly with decreasing fuel-rail pressure, due to decreasing nozzle exit velocity [5, 42]. Higher jet velocities and improved atomization may be caused by enhanced cavitation during the needle closing process [43]. Further studies are required to investigate this phenomenon. However, it should also be noted that particularly large droplets were observed at the very end of injection, when the discharge velocity collapses [5, 33, 34, 44, 45]. This condition is not yet reached in the data presented in Fig. 9, as noted previously.

In Fig. 10, a 2D mapping of the extinction coefficient measured with dual-SLIPI is shown. In this case, the illuminating laser sheet is slightly smaller than for the LIF/Mie ratio and equals 27 mm in height instead of 33 mm. By definition, the extinction coefficient, μ_e, corresponds to the product of the droplet number density N times the extinction cross section, σ_e (which is directly related to the droplets size). Therefore, for a hypothetical monodisperse spray, a mapping of the extinction coefficient provides a relative distribution of droplets concentration. It can be observed from these results that the extinction coefficient reduces by a factor of ~ 2 between 2,000 and 3,000 μs. This confirms that the spray becomes more dilute in the course of the needle closing process. Note that the corresponding injection rate is decreasing smoothly and nearly linearly in this phase. The effect of evaporation is expected to be weak at this time scale, due to the room ambient temperature. It is reported that the vapor pressure for n-decane at room temperature is 130 Pa [46]. In addition, evaporation is expected to be particularly slow in the core of the spray, because it is likely mixing limited there [47]. It should also be pointed out that tracer-based LIF measurements of the fuel volume fraction in sprays are often

Fig. 10 Two-dimensional mapping of a non-reacting diesel spray, showing the distribution of the extinction coefficient at late time after injection start (between 2,000 and 3,000 μs). Extinction coefficient up to 0.45 mm^{-1} is measured. Higher values of μ_e are expected at earlier times. Note that the spray is illuminated from the *right side*
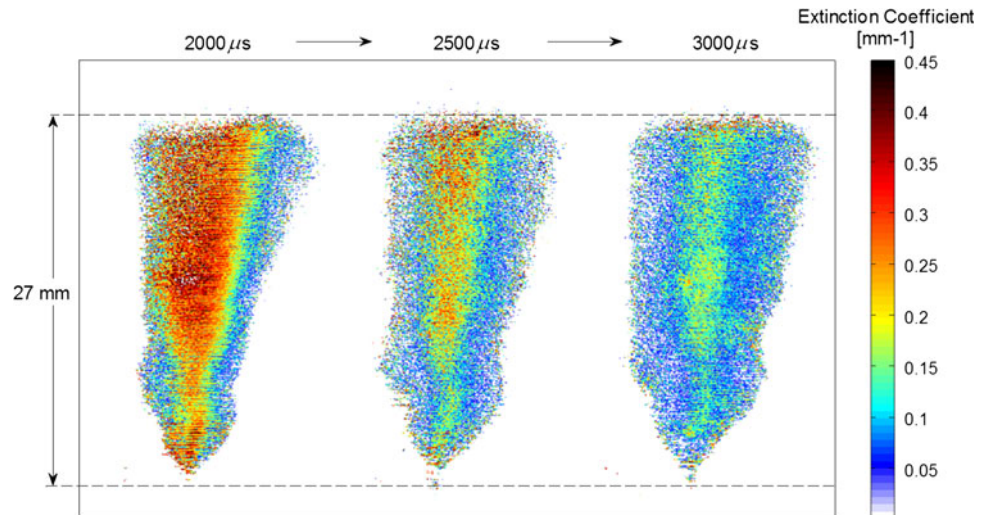
affected by preferential evaporation, i.e., decomposition of the fuel/tracer mixture incurred by the boiling characteristics of these components [48]. However, recent research indicated that preferential evaporation is negligible in diesel sprays under engine-like conditions, due to the rapid evaporation process [48, 49]. This also implies that a wide variety of fuel/tracer mixtures could be used, as suggested in [49].

By accurately calibrating results from SLIPI-LIF/Mie and using results from dual-SLIPI, for the same field of view and at same recording times, it is believed that 2D measurements of both droplets size and concentration could be obtained along the central plane of the diesel spray. These measurements, if applied at short successive times, could lead to the determination of the fuel evaporation rate.

One remarkable benefit of the two complementary approaches presented in this article, is that they both account for laser extinction and signal attenuation as they are based on intensity ratio. As a result, spray symmetry, which is not observable from the direct SLIPI images, can be observed from both the SMD and the extinction coefficient results. However, this becomes questionable in areas where the signal to noise ratio is too low (as observed on the left side of most SLIPI images). In this case, a division of light intensities is not reliable anymore and image thresholding is required (as seen for the 2,000 μs detection case). The optimization of the camera dynamic range is then of important concern when operating SLIPI in highly scattering media, where strong exponential light reduction occurs. Note that information related to at least a third of the spray can still be extracted even at short time after injection start. Also, using a detection system with much larger dynamic range, information on the left side of the spray could be accessible. Finally, another solution would be used fo r counter propagating laser sheets.

6 Conclusion

Structured laser illumination planar imaging was, for the first time, applied to extract quantitative data from a non-reacting diesel spray. The technique was combined with the well-known LIF/Mie planar droplet sizing and with a recent method called dual SLIPI. Results of both droplet SMD and extinction coefficient could be extracted by the respective approaches, without large errors introduced by multiple light scattering. It is believed that such complementary information could lead, in a near future, to the extraction of droplet number density. This would allow the complete and rapid 2D characterization of diesel sprays. As reacting diesel sprays are less optically dense than the non-reacting ones, due to fast evaporation, application in such conditions seems promising, especially for the dual-SLIPI measurements.

References

1. P. Adomeit, H. Rohs, T. Körfer, H. Busch, in *Conference on Thermo- and Fluid Dynamic Processes in Diesel Engines*, Valencia, Sept 2006, pp. 13–15
2. S. Singh, R.D. Reitz, M.P.B. Musculus, T. Lachaux, Combust. Sci. Technol. **179**, 2381 (2007)
3. M. Gauding, T. Brands, C. Felsch, P. Hottenbach, C. Hasse, C. Pauls, G. Grünefeld, N. Peters, in *European combustion meeting*, Vienna, Austria (2009)

4. J. E. Dec, SAE Technical Paper Series No. 970873 (1997)
5. G.J. Smallwood, O.L. Gülder, Atomization Spray **10**, 355 (2000)
6. D.G. Talley, J.F. Verdieck, S.W. Lee, V.G. McDonnell, G.S. Samuelsen, Paper AIAA-96-0469, in *Presented at the thirty-fourth aerospace sciences meeting*, Reno, Jan 1996
7. C.N. Yeh, H. Kosaka, T. Kamimoto, in *Proceedings of the 3rd congress on optical particle sizing*, 1993, pp. 355–361
8. G.J. Smallwood, O.L. Gülder, D.R. Snelling, in *Twenty-fifth symposium (international) on combustion*, 1994, pp. 371–379
9. M.C. Jermy, D.A. Greenhalgh, Appl. Phys. B **71**, 703 (2000)
10. E. Kristensson, L. Araneo, E. Berrocal, J. Manin, M. Richter, M. Aldén, M. Linne, Opt. Express **19**, 13647 (2011)
11. M. Paciaroni, M. Linne, Appl. Opt. **43**, 5100 (2004)
12. D. Sedarsky, E. Berrocal, M. Linne, Opt. Express **19**, 1866 (2011)
13. M. Linne, M. Paciaroni, T. Hall, T. Parker, Exp. Fluids **40**, 836 (2006)
14. C.F. Powell, S.A. Ciatti, S.K. Cheong, J. Liu, J. Wang, SAE Int. J. Fuels Lubr., Series No. 2004-01-2011 (2004)
15. A. Kastengren, C.F. Powell, Z. Liu, J. Wang, SAE Int. J. Fuels Lubr., Series No. 2009-01-0840 (2009)
16. Z. Liu, K. Im, X. Xie, Y. Wang, K. Fezzaa, M.C. Lai, J. Wang, in *11th international conference on liquid atomization and spray systems*, paper 155, Vail, Colorado (2009)
17. C.F. Powell, A.L. Kastengren, Z. Liu, K. Fezzaa, J. Eng. Gas Turbines Power **133**, 012802 (2011)
18. M. Linne, Exp. Fluids **52**, 1251 (2011)
19. J.E. Labs, T.E. Parker, Appl. Opt. **44**, 6049 (2005)
20. J. Labs, T. Parker, Atomization Sprays **16**, 843 (2006)
21. E. Berrocal, E. Kristensson, M. Richter, M. Linne, M. Aldén, Opt. Express **16**, 17870 (2008)
22. E. Kristensson, E. Berrocal, M. Aldén, Opt. Lett. **36**, 1656 (2011)
23. R. Wellander, E. Berrocal, E. Kristensson, M. Richter, M. Aldén, Meas. Sci. Technol. **22**, 125303 (2011)
24. E. Berrocal, J. Johnsson, E. Kristensson, M. Alden, J. Eur. Opt. Soc. Rap. Publ. **7**, 12015 (2012)
25. C. Pauls, S. Vogel, G. Grünefeld, N. Peters, SAE 2007 transactions, J Fuels Lubr., Series No. 2007-01-0020 (2007)
26. M. Cardenas, P. Hottenbach, R. Kneer, G. Grünefeld, SAE Int. J. Engines **2**, 272 (2010)
27. W. Egler, R.J. Giersch, F. Boecking, J. Hammer, J. Hlousek, P. Mattes, U. Projahn, W. Urner, B. Janetzky, Fuel injection systems, in *Handbook of diesel engines*, ed. by K. Mollenhauer, H. Tschoeke (Springer, Berlin, 2010), p. 127
28. R. Domann, Y. Hardalupas, Part. Part. Syst. Charact. **20**, 209 (2003)
29. G. Charalampous, Y. Hardalupas, Appl. Opt. **50**, 1197 (2011)
30. G. Charalampous, Y. Hardalupas, Appl. Opt. **50**, 3622 (2011)
31. E. Berrocal, D. Sedarsky, M. Paciaroni, I. Meglinski, M. Linne, Opt. Express **15**, 10649 (2007)
32. T. Kamimoto, in *International symposium COMODIA*, Yokohama, Japan (1994), pp. 33–41
33. E. Berrocal, E. Kristensson, D. Sedarsky, M. Linne, in *11th international conference on liquid atomization and spray systems*, paper 136, Vail, Colorado (2009)
34. J.-S. Han, P.-H. Lu, X.-B. Xie, M.-C. Lai, N.A. Henein, SAE Technical Papers Series No. 2002-01-2775 (2002)
35. C. Yeh, H. Kosaka, T. Kamimoto, Measurement of drop sizes in unsteady dense sprays, in *Recent advances in spray combustion: spray atomization and drop burning phenomena*, vol 1, American Institute of Aeronautics and Astronautics, Reston (1996)
36. K.D. Kihm, D.P. Terracina, J.A. Caton, J. Inst. Energy **68**, 57 (1995)
37. K.D. Khim, D.P. Terracina, S.E. Payne, J.A. Caton, J. Inst. Energy **67**, 2 (1994)
38. J. Lacoste, C. Crua, M. Heikal, D. Kennaird, M. Gold, SAE Technical Paper Series No. 2003-01-3085 (2003)
39. T. Brands, P. Hottenbach, H.-J. Koß, G. Grünefeld, S. Pischinger, in *15th international symposium on applications of laser techniques to fluid mechanics*, Series No. 2-5-3, Lisbon, Portugal (2010)
40. S. Baik, J. Blanchard, M. Corradini, SAE Technical Paper Series No. 2001-01-0528 (2001)
41. A.H. Lefebvre, *Atomization and Sprays* (Hemisphere Publishing Corporation, New York, 1989)
42. R. Payri, L. Araneo, J. Shakal, V. Soare, J. Mech. Sci. Technol. **22**, 1620 (2008)
43. D.P. Schmidt, M.L. Corradini, Int. J. Engine Res. **2**, 1 (2001)
44. T.C. Wang, J.-S. Han, X.-B. Xie, M.-C. Lai, N.A. Henein, E. Schwarz, W. Bryzik, J. Eng. Gas Turbines Power **125**, 412 (2003)
45. J.B. Blaisot, J. Yon, Exp. Fluids **39**, 977 (2005)
46. D.L. Siebers, SAE Technical Paper Series No. 1999-01-0528 (1999)
47. D. Han, R.R. Steeper, SAE Technical Paper Series No. 2002-01-0837 (2002)
48. P. Hottenbach, T. Brands, G. Grünefeld, SAE Int. J. Engines **4**, 800 (2011)
49. P. Hottenbach, T. Brands, T. Hülser, G. Grünefeld, SAE Technical Paper Series No. 2011-01-1825 (2011)